

Spatial Covariance Constraints for Gaussian Mixture Models

Hanzhang Lu*, Keiran Malott, Venkat Suprabath Bitra, Kirsty Milligan,
 Sanjeena Subedi, Edana Cassol, Vinita Chauhan,
 Connor McNairn, Bryan Muir, Prarthana Pasricha,
 Sangeeta Murugkar, Rowan Thomson, Andrew Jirasek, Jeffrey L. Andrews

Abstract

Although extensive research exists in spatial modeling, few studies have addressed finite mixture model-based clustering methods for spatial data. Finite mixture models, especially Gaussian mixture models, particularly suffer from high dimensionality due to the number of free covariance parameters. This study introduces a spatial covariance constraint for Gaussian mixture models that requires only four free parameters for each component, independent of dimensionality. Using a coordinate system, the spatially constrained Gaussian mixture model enables clustering of multi-way spatial data and inference of spatial patterns. The parameter estimation is conducted by combining the expectation-maximization (EM) algorithm with the generalized least squares (GLS) estimator. Simulation studies and applications to Raman spectroscopy data are provided to demonstrate the proposed model.

1 Introduction

In recent years, the structure of data has grown increasingly complex, characterized by a proliferation of information and greater dimensionality. Spatial correlation, a natural phenomenon that refers to the relationship between values and locations of a variable, is common in various datasets. In modeling spatial patterns, well-established methods such as the Poisson point process (Streit, 2010), Kriging (Oliver and Webster, 1990), and the Matérn covariance function (Genton, 2001) have been proposed and developed. However, in the realm of mixture model-based clustering, there is a limited amount of literature. To the best of our knowledge, the work presented by Lee et al. (2025) is the sole contribution that integrates a mixture of regression models with a Markov random field to cluster spatial data.

*Corresponding Author: University of British Columbia Okanagan Campus, Kelowna, BC, Canada, V1V 1V7.
 Email: hanzhang.lu@ubc.ca

Moreover, in the real world, space is typically considered to be two-dimensional or three-dimensional, so spatial data is naturally arranged in two- or three-dimensional order. The intrinsic structure of spatial data also makes it a part of multi-way data analysis, which has garnered considerable attention in recent years. In terms of the model-based clustering, many matrix variate approaches (Viroli, 2011; Doğru et al., 2016; Gallaugher and McNicholas, 2018; Tomarchio et al., 2022) and tensor variate techniques (Mai et al., 2022; Tomarchio et al., 2023) have been proposed. Although the parsimony of these approaches allows for the analysis of relatively high-dimensional data, they are not designed to capture spatial correlations. To foreshadow our motivating real data analysis, consider the images shown in Figure 6. Therein, a clear spatial autocorrelation is present which the previously mentioned matrix-variate models cannot take advantage of in an efficient manner.

To fill this gap, this study introduces a Gaussian mixture model with spatial constraints (Spat-GMM) for clustering multi-way spatial data and inferring spatial patterns. Based on the linear spatial correlation model proposed by Worsley et al. (1991), a novel covariance structure called the sigmoid decay will be introduced. It assumes that the spatial correlation decreases as the Euclidean distance increases, but in a certain range of distance, the correlation decreases dramatically and then stabilizes. With the Euclidean distance evaluated on a given coordinate system, under the sigmoid decay structure, the covariance matrices can be decomposed as a linear combination of three symmetric matrices. This structure enables the model to estimate spatial covariance matrices using only three parameters, thereby preventing parameter inflation as dimensionality increases. To conduct the parameter estimation for the spatial covariance parameters, a variant of the expectation-maximization (EM) algorithm combined with the generalized least squares (GLS) estimator (Browne, 1974) is used.

2 Background

Before introducing the relevant background knowledge, we first introduce the notations and the basic definitions. In the multi-way data scenario, we denote random matrices and tensors as \mathcal{X} and the corresponding realization as \mathcal{X} . In the multivariate case, the random vector is denoted as \mathbf{X} , with \mathbf{x} representing a specific realization. Regarding the scalars, the random variable is denoted by X . Furthermore, suppose we have an M -order random tensor $\mathcal{X} \in \mathbb{R}^{p_1 \times \dots \times p_M}$ along with a coordinate system \mathcal{C} , then the total number of variables can be found as $p = \prod_{m=1}^M p_m$. The vectorization operator $\text{vec}(\cdot)$ transform a tensor \mathcal{X} to a vector $\mathbf{X} = \text{vec}(\mathcal{X}) \in \mathbb{R}^{p \times 1}$, with X_{i_1, \dots, i_M} being its j th element, where $j = 1 + \sum_{m=1}^M (i_m - 1) \prod_{m'=1}^{m-1} p_{m'}$. For an element X_{i_1, \dots, i_m} in \mathcal{X} , or correspondingly X_j in \mathbf{X} , the coordinate can be its subscript (i_1, \dots, i_m) or a one-to-one projection

vector \mathbf{c}_j of (i_1, \dots, i_M) . The coordinate system \mathcal{C} is a set containing the unique corresponding coordinates $\mathbf{c}_1, \dots, \mathbf{c}_p$. For two coordinates \mathbf{c}_i and \mathbf{c}_j , the spatial proximity measured by the Euclidean distance between these two elements is calculated via

$$d_{ij} = \sqrt{(\mathbf{c}_i - \mathbf{c}_j)^2}.$$

A spatial system is defined as the random vector \mathbf{X} and its coordinate system \mathcal{C} .

2.1 Gaussian Mixture Models

Model-based clustering is a statistical method that utilizes finite mixture models, first introduced by [Wolfe \(1963\)](#) and subsequently established in the literature ([McLachlan and Peel, 2000](#); [McNicholas, 2016](#)). A finite mixture model represents the distribution of a heterogeneous population as a combination of several distributions, each corresponding to a homogeneous subpopulation. These subpopulations, known as components, typically follow distributions from a specified family such as Gaussian ([Scrucca et al., 2016](#)), t-distributions ([Andrews and McNicholas, 2012](#)), or generalized hyperbolic distributions ([Browne and McNicholas, 2015](#)).

One of the oldest and most classic finite mixture models for clustering is the Gaussian mixture model (GMM; [Wolfe, 1970](#)), which serves as the foundation for numerous model-based clustering methods. The density function of a p -dimensional, G -component GMM is given by

$$f(\mathbf{x} \mid \boldsymbol{\vartheta}) = \sum_{g=1}^G \pi_g \phi(\mathbf{x} \mid \boldsymbol{\mu}_g, \boldsymbol{\Sigma}_g), \quad (1)$$

where $\phi(\mathbf{x} \mid \boldsymbol{\mu}_g, \boldsymbol{\Sigma}_g)$ is the g th p -dimensional Gaussian density function with the mean vector $\boldsymbol{\mu}_g$ and the covariance matrix $\boldsymbol{\Sigma}_g$ and $\boldsymbol{\vartheta} = \{\pi_1, \dots, \pi_G, \boldsymbol{\mu}_1, \dots, \boldsymbol{\mu}_G, \boldsymbol{\Sigma}_1, \dots, \boldsymbol{\Sigma}_G\}$ represents the parameter space.

Despite its popularity, the GMM faces several challenges, especially in high-dimensional settings. The primary issue is the large number of free parameters required for the component covariance matrices. For the model in equation (1), the number of free covariance parameters is calculated as

$$\frac{1}{2}Gp(p+1),$$

which becomes considerable as the dimensionality p increases.

2.2 Constrained Gaussian Models

To mitigate this issue, researchers have proposed several covariance structures for GMMs that reduce the number of free parameters while better capturing the covariance of data. [Celeux and](#)

Govaert (1995) proposed the Gaussian parsimonious clustering models (GPCM) with an eigen-decomposition of the group covariance matrices,

$$\boldsymbol{\Sigma}_g = \lambda_g \boldsymbol{\Gamma}_g \boldsymbol{\Omega}_g \boldsymbol{\Gamma}_g', \quad (2)$$

where $\lambda_g = |\boldsymbol{\Sigma}_g|^{1/p}$, $\boldsymbol{\Gamma}_g$ contains the eigenvectors of $\boldsymbol{\Sigma}_g$, and $\boldsymbol{\Omega}_g$ is a diagonal matrix of normalized eigenvalues in decreasing order with $|\boldsymbol{\Omega}_g| = 1$. Imposing constraints on these elements reduces the number of free covariance parameters.

As an extension of the factor analysis model (Spearman, 1987), the mixture of factor analyzers model is presented by Ghahramani et al. (1996), which assumes \mathbf{X}_i can be expressed as a mixture of linear combinations of r -dimensional latent factors \mathbf{U}_{ig} , where $r \ll p$, which can be written as

$$\mathbf{X}_i = \boldsymbol{\mu}_g + \boldsymbol{\Lambda}_g \mathbf{U}_{ig} + \boldsymbol{\epsilon}_{ig}, \quad (3)$$

with probability π_g , where g is the index of the corresponding component, $\boldsymbol{\mu}_g$ is the $p \times 1$ location vector of g th group, $\boldsymbol{\Lambda}_g$ is the $p \times r$ factor loadings of g th group, $\mathbf{U}_{ig} \sim \mathcal{N}_r(\mathbf{0}, \mathbf{I}_r)$, and $\boldsymbol{\epsilon}_{ig} \sim \mathcal{N}_p(\mathbf{0}, \boldsymbol{\Psi}_g)$. Here, \mathbf{I}_r refers to a r -dimensional identity matrix, and $\boldsymbol{\Psi}_g = \text{diag}(\psi_{1g}, \psi_{2g}, \dots, \psi_{pg})$ denotes a $p \times p$ diagonal matrix with elements $(\psi_{1g}, \psi_{2g}, \dots, \psi_{pg})$. Under (3), the group covariance can be decomposed as

$$\boldsymbol{\Sigma}_g = \boldsymbol{\Lambda}_g \boldsymbol{\Lambda}_g' + \boldsymbol{\Psi}_g.$$

The number of free covariance parameters in the MFA is given by

$$G \left[pr + p - \frac{1}{2}r(r-1) \right].$$

Hence, the reduction of the total number of free parameters is

$$\frac{1}{2}Gp(p+1) - G \left[pr + p - \frac{1}{2}r(r-1) \right] = \frac{1}{2}G \left[(p-r)^2 - (p+r) \right],$$

which is positive with $(p-r)^2 > (p+r)$. Moreover, by imposing the constraints $\boldsymbol{\Lambda}_g = \boldsymbol{\Lambda}$, $\boldsymbol{\Psi}_g = \boldsymbol{\Psi}$, and $\boldsymbol{\Psi}_g = \boldsymbol{\psi}_g \mathbf{I}$ to allow different components to share covariance parameters, McNicholas and Murphy (2008) propose a family of eight parsimonious Gaussian model, which reduce the number of free parameters in the covariance structure further.

2.3 Mixture of Matrix normal distributions

Another extension of the GMM is the mixture of matrix normal distributions (MMN) proposed by Viroli (2011), which leverages the matrix normal distribution (Gupta and Varga, 1992; Gupta and

[Nagar, 2018](#)) to accommodate matrix-variate inputs. The matrix normal distribution, also known as the matrix Gaussian distribution, is a special case of the multivariate normal distribution that applies to matrix variate random variables. It features two distinct covariance matrices to capture the variability and correlation among the rows and columns, separately.

Suppose a $p \times q$ random matrix \mathcal{X} arises from a matrix Gaussian distribution with a $p \times q$ location matrix \mathbf{M} , a $p \times p$ across-row covariance matrix $\mathbf{\Xi}$ and a $q \times q$ across-column covariance matrix $\mathbf{\Omega}$, denoted by $\mathcal{N}_{p \times q}(\mathbf{M}, \mathbf{\Xi}, \mathbf{\Omega})$, has the density function, for all $\mathcal{X} \subset \mathcal{X}$, can be written as

$$\phi_{p \times q}(\mathcal{X} | \mathbf{M}, \mathbf{\Xi}, \mathbf{\Omega}) = \frac{\exp\left\{-\frac{1}{2} \text{tr}(\mathbf{\Xi}^{-1}(\mathcal{X} - \mathbf{M})\mathbf{\Omega}^{-1}(\mathcal{X} - \mathbf{M})')\right\}}{(2\pi)^{\frac{pq}{2}} |\mathbf{\Xi}|^{\frac{p}{2}} |\mathbf{\Omega}|^{\frac{q}{2}}}. \quad (4)$$

One key property of the matrix normal distribution is an equivalent definition that if $\mathcal{X} \sim \mathcal{N}_{p \times q}(\mathbf{M}, \mathbf{\Xi}, \mathbf{\Omega})$, then $\text{vec}(\mathcal{X}) \sim \mathcal{N}_{pq}(\text{vec}(\mathbf{M}), \mathbf{\Omega} \otimes \mathbf{\Xi})$, where $\mathcal{N}_{pq}(\cdot)$ represents the mp -dimensional multivariate normal distribution, $\text{vec}(\cdot)$ is the vectorization operator, and \otimes is the Kronecker product. Building on this property, the density of a G -component MMN can be written as

$$f(\mathcal{X} | \boldsymbol{\vartheta}) = \sum_{g=1}^G \pi_g \phi_{p \times q}(\mathcal{X} | \mathbf{M}_g, \mathbf{\Xi}_g, \mathbf{\Omega}_g), \quad (5)$$

where $\phi_{p \times q}(\mathcal{X} | \mathbf{M}_g, \mathbf{\Xi}_g, \mathbf{\Omega}_g)$ denotes the g th matrix-variate Gaussian density function, characterized by the mean matrix \mathbf{M}_g , the across-row covariance matrix $\mathbf{\Xi}_g$, and the across-column covariance matrix $\mathbf{\Omega}_g$. Thus, the MMN can be interpreted as the multivariate GMM with a Kronecker product covariance structure. The Kronecker product decomposes the component covariance matrices into two positive definite matrices, which separately handle the covariance across rows and columns. Besides, this approach also eases the dimensionality challenge associated with the covariance matrices in the multivariate GMM. Specifically, the reduction of the free covariance parameters is

$$\frac{1}{2}G[pq(pq + 1) - p(p + 1) - q(q + 1)],$$

which is strictly positive.

2.4 Linear Spatial Covariance Structure

The linear spatial covariance structure, or the linear spatial correlation model, proposed by [Worsley et al. \(1991\)](#) provides an efficient way to model spatial patterns. As a special case of the linear covariance structures discussed by [Browne \(1974\)](#), it assumes a spatial covariance matrix can be decomposed as a linear combination of three predefined matrices. Suppose we have a p -dimensional spatial system \mathbf{X} following Gaussian distribution with covariance matrix $\mathbf{\Sigma}$ and its coordinate

system \mathcal{C} , the linear spatial covariance suggests that the covariance

$$\boldsymbol{\Sigma} = \alpha_1 \mathbf{J} - \alpha_2 \mathbf{D} + \alpha_3 \mathbf{I}, \quad (6)$$

where $\boldsymbol{\Sigma}$ is the covariance matrix of \mathbf{X} , $\alpha_1, \alpha_2, \alpha_3 \in \mathbb{R}_+$ are the linear spatial parameters, \mathbf{J} is a $p \times p$ matrix of ones, \mathbf{D} is a $p \times p$ matrix of the Euclidean distance evaluated on \mathcal{C} , and \mathbf{I} is a $p \times p$ identity matrix. With the distance d_{ij} between the i th and j th elements X_i and X_j , their covariance σ_{ij} can be calculated via

$$\sigma_{ij} = \begin{cases} \alpha_1 - \alpha_2 d_{ij}^2 & \text{if } i \neq j, \\ \alpha_1 + \alpha_3 & \text{if } i = j. \end{cases} \quad (7)$$

The function (7) suggests that the spatial covariance decreases quadratically with the Euclidean distance, so this structure is also called the quadratic decay (QD) covariance structure. Moreover, in (6), except for three predefined matrices, there are only three free parameters. As the dimensionality increases, these three matrices will be expanded, but this will not affect the number of free parameters the QD uses. Hence, the principal advantage of this structure lies in its ability to model a spatial covariance matrix with only three parameters, regardless of dimensionality.

In terms of parameter estimation, Browne (1974) presents the generalized least squares (GLS) estimator for estimating the linear covariance structure. Suppose that a set of p -dimensional random vectors, denoted as \mathbf{X}_i for $i = 1, 2, \dots, N$ identically, independently follow $\mathcal{N}(\boldsymbol{\mu}, \boldsymbol{\Sigma})$, with a shared coordinate system \mathcal{C} . Under the quadratic decay, $\boldsymbol{\Sigma}$ follows (6). The GLS estimates $\hat{\alpha}_1, \hat{\alpha}_2, \hat{\alpha}_3$ by minimizing the quadratic form of the residual as follows

$$g(\boldsymbol{\alpha}) = \frac{1}{2} (\mathbf{s} - \boldsymbol{\Delta}\boldsymbol{\alpha})' (\mathbf{V} \otimes \mathbf{V})^{-1} (\mathbf{s} - \boldsymbol{\Delta}\boldsymbol{\alpha}), \quad (8)$$

where $\boldsymbol{\alpha} = (\alpha_1, \alpha_2, \alpha_3)'$ is the vector of the linear spatial covariance parameter, $\mathbf{s} = \text{vec}(\mathbf{S})$ is the vectorization of the sample covariance matrix, $\boldsymbol{\Delta}$ is the design matrix with the columns $\text{vec}(\mathbf{J}), -\text{vec}(\mathbf{D}), \text{vec}(\mathbf{I})$, and \mathbf{V} is the positive definite weight matrix. Since the linear spatial covariance structure is a special case of the linear covariance structure, the GLS estimator can also estimate $\alpha_1, \alpha_2, \alpha_3$ in (6). There are several desirable properties the GLS estimator possesses, but one worth noting here is that the GLS estimates are also the maximum likelihood estimates (MLE), which are also the minimizers of

$$F = \log |\boldsymbol{\Xi}| - \log |\mathbf{S}| + \text{tr} \{ \mathbf{S} \boldsymbol{\Xi}^{-1} \} - p.$$

3 Methodology

3.1 Covariance Structure

Although the QD covariance structure offers us considerable parsimony, it also imposes some restrictions. Since the matrix \mathbf{D} in (6) is entirely determined by the given coordinate system, when facing different coordinate systems, it always requires different normalizations to keep the distance in a reasonable range. Moreover, in the high-dimensional context, collinearity is a significant issue for the QD structure, which renders the matrix non-positive definite. Therefore, to overcome these concerns, we propose a sigmoid decay (SD) structure by changing the quadratic function applied to the distance to a parameterized sigmoid function. It assumes that the spatial correlation diminishes to a specific value at a certain distance and then stabilizes. The introduced sigmoid function in the SD structure is

$$h(x) = a \left(\frac{1}{1 + e^{-\beta x+3}} - s \right), \quad (9)$$

where $x \leq 2$, $s = \frac{1}{1+e^3}$, $a = (\frac{1}{1+exp(-2\beta+3)} - s)^{-1}$ and β is a tuning parameter. It is worth noting that this function always starts at $(0, 0)$ and passes through $(2, 1)$. Unlike the QD, the distance is always normalized to be in the range of $[0, 2]$ regardless of coordinate systems. In this way, the value of the sigmoid parameter β is kept in the sensitive and appropriate range. Additionally, this function helps prevent collinearity in the linear covariance structure. Figure 1 shows the quadratic

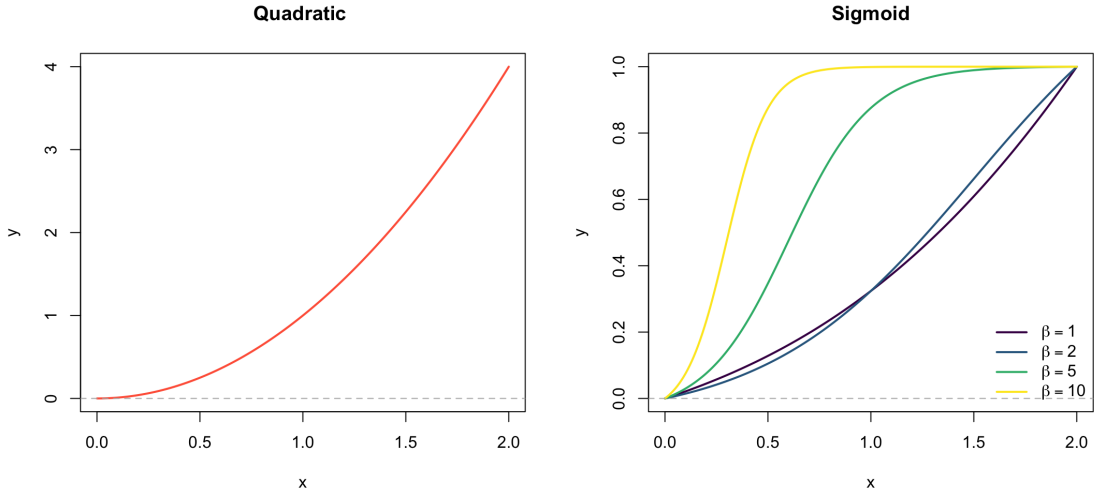


Figure 1: Decay curves for the quadratic (left) and sigmoid (right) models.

curve and the sigmoid curves with different parameters. Except for the function applied to the distance, the rest of the sigmoid decay is similar to the quadratic decay, which can be written as

$$\boldsymbol{\Xi} = \alpha_1 \mathbf{J} - \alpha_2 \mathbf{D}(\beta) + \alpha_3 \mathbf{I},$$

where $\mathbf{D}(\beta)$ is the only different part. With the distance d_{ij} measured on the coordinate system \mathcal{C} , the element of $\mathbf{D}(\beta)$ at the i th row and the j th column is $h(d_{ij})$. Hence, the element-wise version of the sigmoid decay is

$$\xi_{ij} = \begin{cases} \alpha_1 - \alpha_2 h(d_{ij}) & \text{if } i \neq j, \\ \alpha_1 + \alpha_3 & \text{if } i = j, \end{cases}$$

where ξ_{ij} is the element of Ξ at (i, j) . Three simulated 100×100 matrices are demonstrated in Figure 2 to show the effect on the spatial pattern of the QD and SD covariance structure. From the figure, we can see that the QD simulation image gradually decreases from the lower left to the upper right without any bulge. The SD-simulated image shows multiple obvious small bulges, and each pixel exhibits stronger local spatial positive correlation.

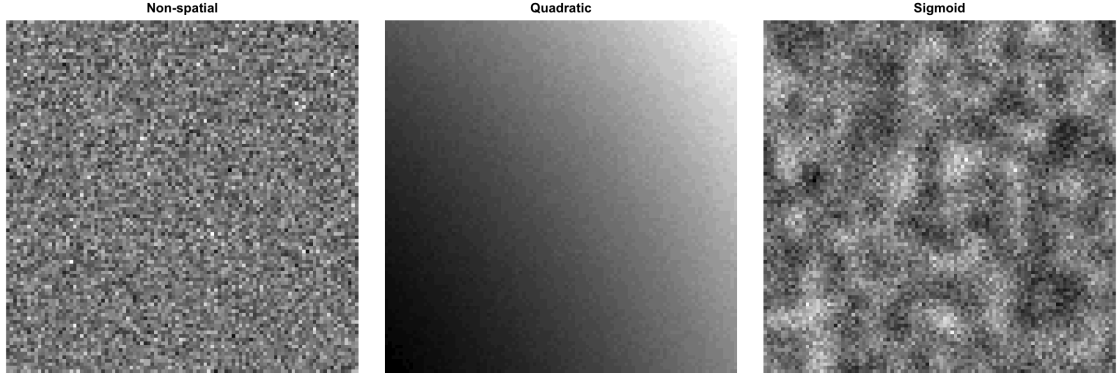


Figure 2: Simulated spatial maps from Gaussian noise (left), quadratic decay (middle), and sigmoid decay (right) models.

3.2 Model Specification

The probability density of a G -component Gaussian mixture model with the sigmoid decay covariance structure (SpatGMM) is

$$f(\mathbf{x} \mid \boldsymbol{\vartheta}) = \sum_{g=1}^G \pi_g \phi(\mathbf{x} \mid \boldsymbol{\mu}_g, \Xi_g), \quad (10)$$

where $\pi_g > 0$, such that $\sum_{g=1}^G \pi_g = 1$, is the g th mixing proportion, $\boldsymbol{\mu}_g$ is the g th group mean vector, Ξ_g is the g th group covariance matrix, ϕ is the p -dimensional multivariate Gaussian density function, and $\boldsymbol{\vartheta} = \{\pi_1, \dots, \pi_G, \boldsymbol{\mu}_1, \dots, \boldsymbol{\mu}_G, \Xi_1, \dots, \Xi_G\}$ is the parameter space. With the coordinate system \mathcal{C} and the sigmoid function $h(d)$, Ξ_g can be expressed as

$$\Xi_g = \alpha_{1g} \mathbf{J} - \alpha_{2g} \mathbf{D}(\beta_g) + \alpha_{3g} \mathbf{I},$$

where $\alpha_{1g}, \alpha_{2g}, \alpha_{3g} \in \mathbb{R}_+$, the (i, j) element in $\mathbf{D}(\beta_g)$ is the value of $h(d_{ij})$ evaluated on distance d_{ij} , which is

$$D_{ij} = h(d_{ij}) = a \left(\frac{1}{1 + e^{-\beta_g d_{ij} + 3}} - s \right), \quad (11)$$

where a and s have the same definition as above, and β_g is the sigmoid parameter.

3.3 Parameter Estimation

For parameter estimation, due to the linear spatial covariance parameter $\boldsymbol{\alpha}_g$ and the sigmoid parameter β_g , the ordinary EM algorithm for the GMM is not sufficient. As mentioned in Section 2.4, the GLS estimates are also MLEs, which allows us to embed the GLS estimator into the EM algorithm. Therefore, a variant of the EM algorithm is employed to perform parameter estimation for the proposed model. Suppose we have the observations $\mathbf{x}_1, \mathbf{x}_2, \dots, \mathbf{x}_N$, which share a common coordinate system \mathcal{C} . Considering the corresponding latent component membership $\mathbf{z}_1, \mathbf{z}_2, \dots, \mathbf{z}_N$, the complete-data log-likelihood function is

$$\ell_c(\boldsymbol{\vartheta}) = \sum_{i=1}^N \sum_{g=1}^G z_{ig} [\log \pi_g + \log \phi(\mathbf{x}_i \mid \boldsymbol{\mu}_g, \boldsymbol{\Xi}_g)]. \quad (12)$$

E-step: In the E-step, the conditional expectation of (12) is calculated and used for estimating the latent membership \mathbf{z} . Given the estimates of distribution parameters, the update equation of $\hat{\mathbf{z}}$ is

$$\hat{z}_{ig} = \frac{\hat{\pi}_g \phi(\mathbf{x}_i \mid \hat{\boldsymbol{\mu}}_g, \hat{\boldsymbol{\Xi}}_g)}{\sum_{h=1}^G \hat{\pi}_h \phi(\mathbf{x}_i \mid \hat{\boldsymbol{\mu}}_h, \hat{\boldsymbol{\Xi}}_h)},$$

for $i = 1, \dots, N$ and $g = 1, \dots, G$.

M-step 1: In the first M-step, the mixing proportions π_g , and the component means $\boldsymbol{\mu}_g$ are estimated first with conditioning on the estimated latent membership \hat{z}_{ig} . By substituting the estimated latent membership into the complete log-likelihood, the complete-data log-likelihood is

$$\ell_c^{(2)}(\boldsymbol{\vartheta}) = C + \sum_{g=1}^G N_g \log \pi_g - \frac{1}{2} \sum_{g=1}^G \hat{z}_{ig} \text{tr} \left\{ (\mathbf{x}_i - \boldsymbol{\mu}_g)(\mathbf{x}_i - \boldsymbol{\mu}_g)' \hat{\boldsymbol{\Xi}}_g^{-1} \right\},$$

where $N_g = \sum_{i=1}^N \hat{z}_{ig}$. By calculating the derivative of the log-likelihood function and setting it equal to zero, the update equations for $\hat{\pi}_g$ and $\hat{\boldsymbol{\mu}}_g$ separately are

$$\hat{\pi}_g = \frac{N_g}{N}, \quad \hat{\boldsymbol{\mu}}_g = \frac{1}{N_g} \sum_{i=1}^N \hat{z}_{ig} \mathbf{x}_i.$$

M-step 2: In the second M-step, the marginal log-likelihood with respect to Ξ_g is

$$\begin{aligned}
\ell_c^{(3)}(\vartheta) &= C - \frac{1}{2} \sum_{g=1}^G N_g \log |\Xi_g| - \frac{1}{2} \sum_{g=1}^G N_g \operatorname{tr} \{ \mathbf{S}_g \Xi_g^{-1} \} \\
&= C - \frac{1}{2} \sum_{g=1}^G N_g \log |\alpha_{1g} \mathbf{J} - \alpha_{2g} \mathbf{D}(\beta_g) + \alpha_{3g} \mathbf{I}| \\
&\quad - \frac{1}{2} \sum_{g=1}^G N_g \operatorname{tr} \{ \mathbf{S}_g (\alpha_{1g} \mathbf{J} - \alpha_{2g} \mathbf{D}(\beta_g) + \alpha_{3g} \mathbf{I})^{-1} \}
\end{aligned} \tag{13}$$

where C is a constant in terms of Ξ_g , and

$$\mathbf{S}_g = \frac{1}{N_g} \sum_{i=1}^N \hat{z}_{ig} (\mathbf{x}_i - \boldsymbol{\mu}_g) (\mathbf{x}_i - \boldsymbol{\mu}_g)'.$$

Because the GLS estimators can provide us with MLE solutions, maximizing (13) is equivalent to minimizing

$$g(\boldsymbol{\alpha}) = \frac{1}{2} (\mathbf{s}_g - \boldsymbol{\Delta}_g \boldsymbol{\alpha})' (\mathbf{V}^* \otimes \mathbf{V}^*) (\mathbf{s}_g - \boldsymbol{\Delta}_g \boldsymbol{\alpha}), \tag{14}$$

where \mathbf{s}_g is the vectorization of \mathbf{S}_g , $\boldsymbol{\Delta}_g$ is the design matrix which columns are $\operatorname{vec}(\mathbf{J})$, $\operatorname{vec}(\mathbf{D}(\hat{\beta}_g))$, $\operatorname{vec}(\mathbf{I})$, and $\mathbf{V}^* = \{\hat{\Xi}_g^*\}^{-1}$, where $\hat{\Xi}_g^*$ is the estimated covariance matrix calculated in the previous EM iteration. By setting the first derivative of (14) equal to zero, we get the update equation

$$\hat{\boldsymbol{\alpha}}_g = \{\boldsymbol{\Delta}_g' (\mathbf{V}^* \otimes \mathbf{V}^*) \boldsymbol{\Delta}_g\}^{-1} \boldsymbol{\Delta}_g' \operatorname{vec}(\mathbf{V}^* \mathbf{S}_g \mathbf{V}^*). \tag{15}$$

M-step 3: In the last M-step, with $\hat{\boldsymbol{\alpha}}_g$, to estimate the sigmoid parameter β_g , we minimize

$$F_g = \log |\Xi_g| - \log |\mathbf{S}_g| + \operatorname{tr} \{ \mathbf{S}_g \Xi_g^{-1} \} - p, \tag{16}$$

where $\Xi_g = \hat{\alpha}_{1g} \mathbf{J} - \hat{\alpha}_{2g} \mathbf{D}(\beta_g) + \hat{\alpha}_{3g} \mathbf{I}$, with respect to β_g . Minimizing (16) is equivalent to maximizing the likelihood function, so it aligns with the EM algorithm framework. Because of the complexity of the sigmoid function (9), (16) is difficult to optimize. Hence, we use `optimize` in R to compute the solution.

4 Numerical Experiments and Analysis

Three simulation studies are presented to evaluate the performance of the proposed model. Furthermore, the methodology is applied to Raman spectroscopy (RS) data to demonstrate its capacity in practical scenarios. For all simulation studies and the real data application in this section, the coordinate system is defined by the subscripts of the spatial system. But it is also possible to

specify a particular coordinate system. In addition, as discussed in Section 3.1, we normalize the Euclidean distance evaluated on the given coordinate system to be in the range $[0, 2]$. In the following simulation studies and real data analysis, the normalization is always performed. The classification accuracy is evaluated using the adjusted Rand index (ARI; [Hubert and Arabie, 1985](#)), which is an improvement over the Rand index (RI; [Rand, 1971](#)).

4.1 Simulation Studies

Three Monte Carlo simulation studies are conducted to evaluate different aspects of the proposed mixture models. The first simulation design is conducted to demonstrate the effectiveness of spatial parameters α_g and β_g . In different groups, only the spatial parameters being tested will vary, while all other parameters will remain the same. The second numerical experiment aims to demonstrate the capacity of the Bayesian information criterion (BIC; [Schwarz, 1978](#)) to detect the correct specification of the number of components, G . In the third simulation design, MCLUST ([Scrucca et al., 2016](#)), PGMM, and MMN are compared with the proposed approach to demonstrate its superior performance on spatial data.

4.1.1 Simulation Design I - Parameter Recovery

In the first setting, the number of groups is $G = 3$, with the mixing proportions $(\pi_1, \pi_2, \pi_3) = (0.2, 0.3, 0.5)$. Each generated observation is a tensor of order three, with dimensions $5 \times 5 \times 5$ and all the group means are tensors of 0s. The setting of spatial parameters α_g and β_g is shown in Table 1. Aside from α_g and β_g , all the means in each group are shared to be the same. 50 datasets of size $N = 1000$ are generated from the proposed model. Figure 3 shows the visualization of the generated tensors from the three groups, which are difficult to classify with only the naked eye.

Table 1: True spatial parameters associated with each group in simulation design I.

Group	α_{1g}	α_{2g}	α_{3g}	β_g
1	4	3	2	4
2	2	1	1	4
3	4	3	2	10

The result of parameter recovery is illustrated in Table 2, which is accurate with acceptable standard errors. With respect to the clustering performance, the average of ARI for each repeat is 0.98.

4.1.2 Simulation Design II - Model Selection

In this study, to detect the capacity of BIC to select the correct number of components, we set 4 groups with the dimensionality $5 \times 5 \times 5$, still with the mixing proportion $(\pi_1, \pi_2, \pi_3) = (0.2, 0.3, 0.5)$.

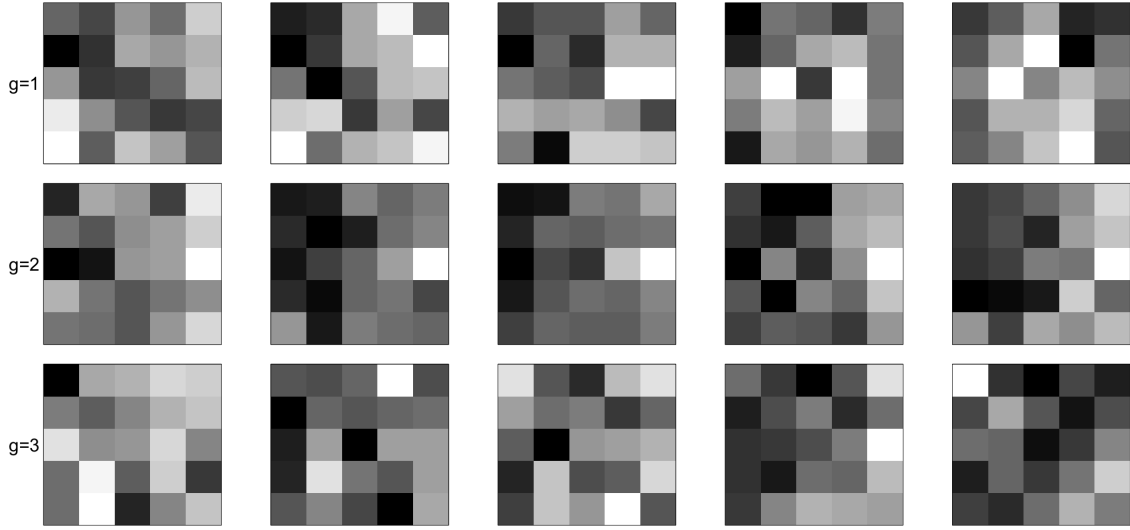


Figure 3: Visualization of the first observed tensor from each of the three groups in simulation design I.

Table 2: Estimated means and standard errors (Se) of $\hat{\alpha}_g$ and $\hat{\beta}_g$ for simulation design I.

Group	$\hat{\alpha}_{1g}$		$\hat{\alpha}_{2g}$		$\hat{\alpha}_{3g}$		$\hat{\beta}_g$	
	Mean	Se	Mean	Se	Mean	Se	Mean	Se
1	3.92	0.133	2.94	0.130	1.97	0.051	4.00	1.848
2	2.02	0.113	1.03	0.120	1.01	0.047	4.00	0.908
3	3.99	0.111	2.99	0.061	2.00	0.034	10.01	0.108

For the location tensors, the four groups have different settings, which are the tensors of 0, 5, 10, and -5 . The setting of the covariance parameter is shown in Table 3. Given the parameter setting,

Table 3: True spatial parameters associated with each group in simulation design II.

Group	α_{1g}	α_{2g}	α_{3g}	β_g
1	4	3	2	4
2	2	1	1	4
3	4	3	2	10
4	1	1	1	10

we generate 50 datasets from our proposed model, each of size 1000. Table 4 shows the best model setting with the highest BIC in all 50 repeats.

Table 4: Model selection performance via the BIC for SpatGMM for simulation design II. True number of components is 4.

	$G = 2$	$G = 3$	$G = 4$	$G = 5$	$G = 6$
Frequency	0	0	38	12	0

4.1.3 Simulation Design III

In the third simulation, we compare the proposed model to MCLUST, PGMM, and MMN. 30 datasets are generated, which follow the probability density (10) with $G = 3$. In each dataset, the shape of the observations is 10×10 , but the setting of the distribution parameter is the same as in Section 4.1.1. For MCLUST, according to the BIC score, the ‘EEE’ model is selected, but the average ARI of 30 repeats is 0, which indicates that MCLUST barely works for the simulated datasets. In terms of the covariance structure of PGMM, since our spatial covariance structure is isotropic, it is reasonable to choose the ‘CUU’ model, which is also what the BIC suggests. Furthermore, the range of the potential number of factors is $\{9, 10, 11, 12, 13\}$, and we use the BIC to select the best model.

Table 5: Clustering performance of four competing models for simulation design III.

	SpatGMM	MCLUST	PGMM	MMN
Average ARI	0.98	0.00	0.47	0.46
Standard deviation of ARI	0.0066	0.0014	0.0316	0.0412

Table 6: BIC of four competing models for simulation design III.

	SpatGMM	MCLUST	PGMM	MMN
Average BIC	-181,898	-405,012	-381,437	-382,563
Standard deviation of BIC	1,541	1,299	1,572	1,546

Based on Tables 5 and 6, we see that for data with spatial covariance, the proposed model is the most appropriate choice.

4.2 Real Application

Following simulated experiments, the performance of the spatially constrained Gaussian mixture model(SpatGMM) is evaluated using Raman spectroscopy data. Raman spectroscopy (RS) measures relative molecular abundances and dynamics. Using a microscope platform, RS can provide spatial resolution on the order of micrometers (Mulvaney and Keating, 2000; Das and Agrawal, 2011; Orlando et al., 2021). The Raman spectra analyzed in this study were obtained from measurements on a radiochromic dosimeter called EBT-3 film (McNairn et al., 2025). Upon exposure to ionizing radiation, the active layer between two matte polyester layers undergoes polymerization, resulting in a stable color change proportional to the absorbed dose (Borca et al., 2013). RS provides a non-invasive, high-resolution approach for detecting polymerization in EBT-3 films by monitoring peaks associated with dose-dependent changes, as shown in Figure 4.

Data were collected from a 0.3 cm square region of interest (ROI) containing an array of 400 distinct sub-ROIs, as illustrated in Figure 5. In our analysis, each sub-ROI is treated as a matrix-

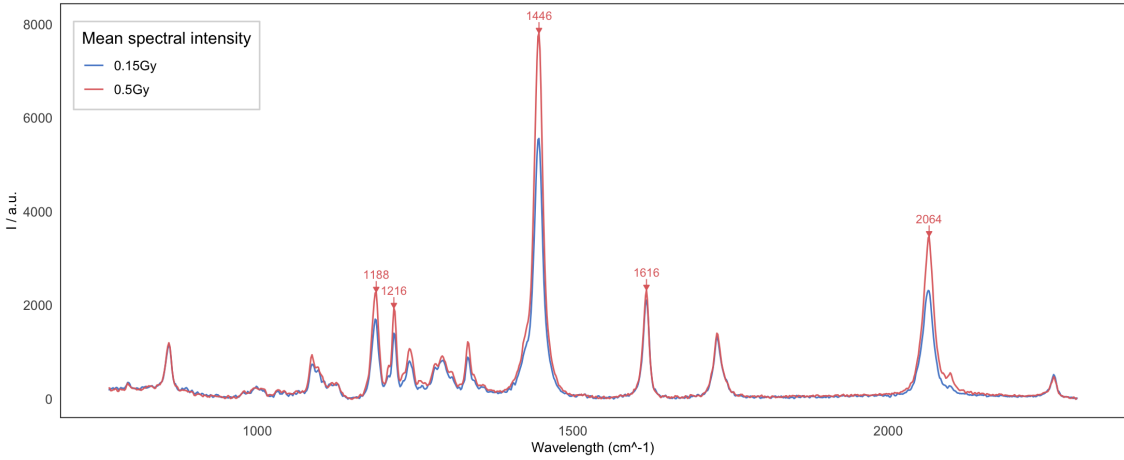


Figure 4: Raman spectra of dosimetric film at two different dosage levels.

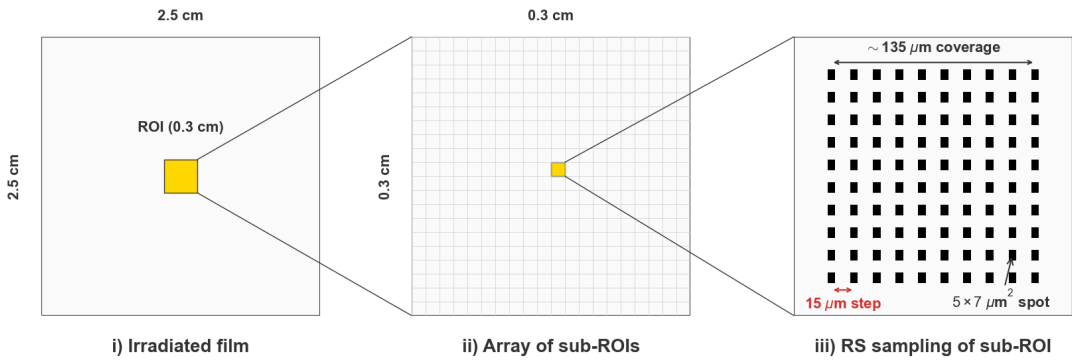


Figure 5: Schematic representation of the RS sampling protocol. (i) Macroscopic view of the irradiated EBT-3 film (2.5×2.5 cm). (ii) The ROI comprises an array of 400 separate sub-ROIs (grids) arranged in a 20×20 pattern. (iii) Microscopic view of a sub-ROI, illustrating the 10×10 point-scan geometry.

variate observation. Each observation consists of a 10×10 point-scan grid acquired with a $15\mu\text{m}$ step size and a $5 \times 7\mu\text{m}^2$ spot size, providing a spatial coverage of approximately $135 \times 135\mu\text{m}^2$. The dataset comprises 800 such observations (totaling 80,000 spectra) collected from two films exposed to radiation doses of 0.15 Gy and 0.50 Gy, respectively. The spectra were recorded over a wavenumber range of 764 to 2300 cm^{-1} . For the spatial analysis, we selected the dose-dependent peak at 2064 cm^{-1} , as highlighted in Figure 4. Representative tensor observations for both dose levels are visualized in Figure 6.

The estimated spatial parameters for the two groups corresponding to the two absorbed dose magnitudes are illustrated in Table 8. Figure 7 displays the sigmoid function with these estimated parameters. In Figure 6, we can easily see that the two groups are very different from each other in magnitude. Therefore, clustering the spectra on the basis of their dose level is a straightforward problem that can be effectively solved by most clustering techniques. Hence, we centralize the data within each dosage level. The proposed model can still accurately capture the covariance and

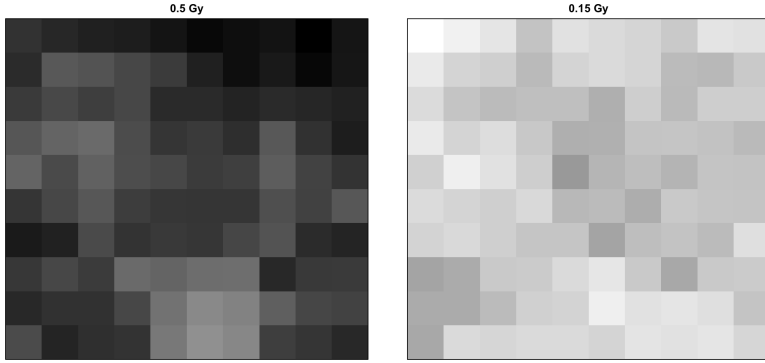


Figure 6: Visualization of a Raman peak at 2064 cm^{-1} measured on a 10×10 grid across two dosimetric films exposed to different radiation levels (0.5 Gy left, 0.15 Gy right).

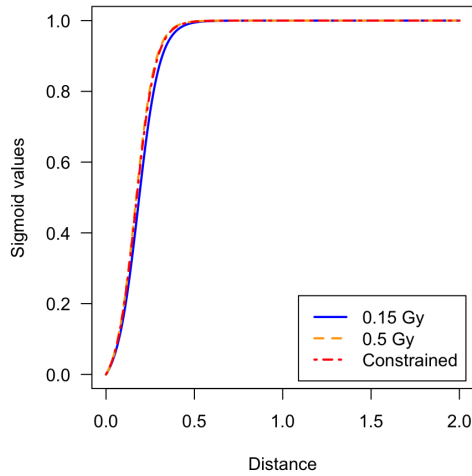


Figure 7: Estimated sigmoid functions in application to dosimetric films data.

group structure of the centered data, but MCLUST and MMN no longer work. Regarding PGMM, we set the number of factors to be in the range of 4 to 16 and use the BIC to select the best model. According to the BIC, the ‘CUC’ model with 16 factors is selected. Although the PGMM model achieves good clustering accuracy, as shown in Table 7, it has a lower BIC score.

Table 7: Comparison of performance between PGMM and SpatGMM on group-centered dosimetric film data.

	ARI	BIC
SpatGMM	0.926	-918,876
PGMM	0.883	-1,081,612

In addition to the clustering results, we also focus on the spatial pattern of the Raman maps. According to the estimated spatial parameters, there is a temptation to think of these parameters as ‘similar’. To assess whether spatial patterns differ significantly, a constrained model is implemented in which all spatial covariance parameters are shared between groups, which is $\alpha_1 = \alpha_2$ and $\beta_1 = \beta_2$. The estimated spatial parameters of the constrained model are also listed in Table 8

for comparison. Table 8 also presents the BIC scores for both the unconstrained and constrained models. As the BIC value for the unconstrained model is higher than that for the constrained

Table 8: Estimated spatial parameters for SpatGMM on dosimetric film data with individual parameters per group (first two rows) and parameters constrained across groups (third row).

Group	$\hat{\alpha}_{1g}$	$\hat{\alpha}_{2g}$	$\hat{\alpha}_{3g}$	$\hat{\beta}_g$	BIC
0.5 Gy	81,364	67,207	20,563	18.1	-919,001
0.15 Gy	33,484	19,415	8,958	16.5	
Constrained	57,584	43,448	14,623	17.8	-930,558

model in Table 8, statistically, we can argue that the spatial polymerization patterns of EBT-3 films at the micron-scales level differ between these two radiation dosages.

5 Summary

A finite Gaussian mixture model with spatial constraints is proposed for clustering tensor variate data that exhibits intrinsic spatial correlation. Given a coordinate system, the covariance matrices can be modeled as sigmoid function values of spatial proximity, which is the sigmoid decay. The proximity within the spatial system is measured by the Euclidean distance between the coordinates, which is then normalized to maintain consistency. The structure can first help us infer the sigmoid-like spatial correlation between elements in the spatial systems of different groups. Furthermore, it offers the finite mixture model substantial parsimony. No matter how large the dimensionality is, this structure can model the covariance matrix with only a constant number of free parameters, which is 5. In addition, along with the GLS estimator, a variant of the EM algorithm is illustrated for parameter estimation.

Although the sigmoid decay structure offers some benefits, there are still aspects of it that require improvement. First, even if the sigmoid decay provides more flexibility than the quadratic decay, it still can be restrictive in some cases, because the sigmoid assumption may also not hold water. It is general to assume that the spatial correlation decreases as the distance increases, but the relationship may not be perfectly sigmoid-like. Therefore, a more flexible framework is required. Second, under the current structure, we also assume the variance of each element in the spatial systems is the same. However, this is not the case in many instances, such as with pixel values in a collection of pictures. Third, the parameter estimation procedure for the sigmoid parameter is not stable. During the optimization procedure for estimating the sigmoid parameter, the corresponding covariance matrix may be singular, which will affect the calculation of the objective function. Moreover, the calculation of the inversion of the covariance matrix remains a problem, despite its well-structured nature. However, suppose the subscripts of the elements are used as the coordinate system. In that case, the covariance matrix is also a Toeplitz block Toeplitz

matrix, which has a special trick for inversion calculations ([Wax and Kailath, 2003](#)).

References

Andrews, J. L. and McNicholas, P. D. (2012). Model-based clustering, classification, and discriminant analysis via mixtures of multivariate t-distributions: the t-EIGEN family. *Statistics and Computing*, 22:1021–1029.

Borca, V. C., Pasquino, M., Russo, G., Grosso, P., Cante, D., Sciacero, P., Girelli, G., Porta, M. R. L., and Tofani, S. (2013). Dosimetric characterization and use of GAFCHROMIC EBT3 film for imrt dose verification. *Journal Applied Clinical Medical Physics*, 14(2):158–171.

Browne, M. W. (1974). Generalized least squares estimators in the analysis of covariance structures. *South African Statistical Journal*, 8(1):1–24.

Browne, R. P. and McNicholas, P. D. (2015). A mixture of generalized hyperbolic distributions. *Canadian Journal of Statistics*, 43(2):176–198.

Celeux, G. and Govaert, G. (1995). Gaussian parsimonious clustering models. *Pattern Recognition*, 28:781–793.

Das, R. S. and Agrawal, Y. (2011). Raman spectroscopy: Recent advancements, techniques and applications. *Vibrational spectroscopy*, 57(2):163–176.

Doğru, F. Z., Bulut, Y. M., and Arslan, O. (2016). Finite mixtures of matrix variate t-distributions. *Gazi University Journal of Science*, 29(2):335–341.

Gallagher, M. P. and McNicholas, P. D. (2018). Finite mixtures of skewed matrix variate distributions. *Pattern Recognition*, 80:83–93.

Genton, M. G. (2001). Classes of kernels for machine learning: a statistics perspective. *Journal of Machine Learning Research*, 2(Dec):299–312.

Ghahramani, Z., Hinton, G. E., et al. (1996). The EM algorithm for mixtures of factor analyzers. Technical report, Technical Report CRG-TR-96-1, University of Toronto.

Gupta, A. and Varga, T. (1992). Characterization of matrix variate normal distributions. *Journal of Multivariate Analysis*, 41(1):80–88.

Gupta, A. K. and Nagar, D. K. (2018). *Matrix variate distributions*. Chapman and Hall/CRC.

Hubert, L. and Arabie, P. (1985). Comparing partitions. *Journal of Classification*, 2:193–218.

Lee, J., Gallaugher, M. P. B., and Hering, A. S. (2025). Clustering spatial data with a mixture of skewed regression models. *Technometrics*, 67(3):505–515.

Mai, Q., Zhang, X., Pan, Y., and Deng, K. (2022). A doubly enhanced EM algorithm for model-based tensor clustering. *Journal of the American Statistical Association*, 117(540):2120–2134.

McLachlan, G. J. and Peel, D. (2000). *Finite mixture models*. John Wiley & Sons.

McNairn, C., Pasricha, P., Milligan, K., Mansour, I. R., Cassol, E., Chauhan, V., Andrews, J. L., Subedi, S., Jirasek, A., Muir, B. R., et al. (2025). Exploring the potential of raman micro-spectroscopy of radiochromic films for experimental microdosimetry. *Medical Physics*, 52(7):e17900.

McNicholas, P. D. (2016). *Mixture model-based classification*. Chapman and Hall/CRC.

McNicholas, P. D. and Murphy, T. B. (2008). Parsimonious Gaussian mixture models. *Statistics and Computing*, 18:285–296.

Mulvaney, S. P. and Keating, C. D. (2000). Raman spectroscopy. *Analytical Chemistry*, 72(12):145–158.

Oliver, M. A. and Webster, R. (1990). Kriging: a method of interpolation for geographical information systems. *International Journal of Geographical Information System*, 4(3):313–332.

Orlando, A., Franceschini, F., Muscas, C., Pidkova, S., Bartoli, M., Rovere, M., and Tagliaferro, A. (2021). A comprehensive review on raman spectroscopy applications. *Chemosensors*, 9(9):262.

Rand, W. M. (1971). Objective criteria for the evaluation of clustering methods. *Journal of the American Statistical Association*, 66(336):846–850.

Schwarz, G. (1978). Estimating the dimension of a model. *The Annals of Statistics*, 6(2):461–464.

Scrucca, L., Fop, M., Murphy, T. B., and Raftery, A. E. (2016). mclust 5: clustering, classification and density estimation using Gaussian finite mixture models. *The R Journal*, 8(1):289.

Spearman, C. (1987). The proof and measurement of association between two things. *The American Journal of Psychology*, 100(3/4):441–471.

Streit, R. L. (2010). The poisson point process. In *Poisson Point Processes: Imaging, Tracking, and Sensing*, pages 11–55. Springer.

Tomarchio, S. D., Gallaugher, M. P., Punzo, A., and McNicholas, P. D. (2022). Mixtures of matrix-variate contaminated normal distributions. *Journal of Computational and Graphical Statistics*, 31(2):413–421.

Tomarchio, S. D., Punzo, A., and Bagnato, L. (2023). Parsimonious mixtures for the analysis of tensor-variate data. *Statistics and Computing*, 33(6):123.

Viroli, C. (2011). Finite mixtures of matrix normal distributions for classifying three-way data. *Statistics and Computing*, 21:511–522.

Wax, M. and Kailath, T. (2003). Efficient inversion of toeplitz-block toeplitz matrix. *IEEE transactions on acoustics, speech, and signal processing*, 31(5):1218–1221.

Wolfe, J. H. (1963). *Object cluster analysis of social areas*. PhD thesis, University of California.

Wolfe, J. H. (1970). Pattern clustering by multivariate mixture analysis. *Multivariate Behavioral Research*, 5:329–350.

Worsley, K., Evans, A., Strother, S., and Tyler, J. (1991). A linear spatial correlation model, with applications to positron emission tomography. *Journal of the American Statistical Association*, 86(413):55–67.